Materials and Design 196 (2020) 109139

Contents lists available at ScienceDirect

Materials and Design

journal homepage: www.elsevier.com/locate/matdes

Aging behavior of Al-Li-(Cu, Mg) alloys processed by different deformation methods

Shuaishuai Qin [a], Seungwon Lee [b,*], Taiki Tsuchiya [b], Kenji Matsuda [b], Zenji Horita [c], Robert Kocisko [d], Tibor Kvackaj [d]

[a] Graduate School of Science and Engineering, University of Toyama, Toyama, Japan
[b] Faculty of Sustainable Design, Department of Materials Design and Engineering, Graduate School of Science and Engineering for Research, University of Toyama, Toyama, Japan
[c] Faculty of Engineering, Department of Materials Science and Engineering, Kyushu University, Fukuoka, Japan
[d] Faculty of Metallurgy, Department of Plastic Deformation and Process Simulations, Technical University of Kosice, Kosice, Slovakia

HIGHLIGHTS

- Cu is more effective than Mg for improving the as-deformed hardness of Al-Li alloy under different equivalent strains (ε).
- Addition of Cu or Mg enhances grain refinement and suppresses grain growth during aging treatment.
- When ε > 30, the addition of Cu or Mg makes the binary Al-Li alloy obtain age- hardenability.
- For Al-Li-Cu alloy, the introduced ε should avoid forming low angle boundaries due to the coarsening of T_1 phase.

GRAPHICAL ABSTRACT

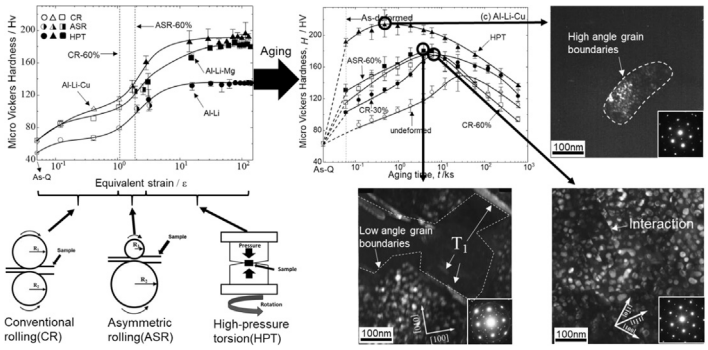

ARTICLE INFO

Article history:
Received 29 May 2020
Received in revised form 8 September 2020
Accepted 8 September 2020
Available online 12 September 2020

Keywords:
Al-Li-(Cu, Mg) alloys
Alloying elements
High-pressure torsion (HPT)
Asymmetric rolling (ASR)
Aging behavior

ABSTRACT

Structural features and aging behavior of Al—Li, Al-Li-Cu and Al-Li-Mg alloys under different equivalent strains (ε) were investigated. Following solid-solution treatment, high-pressure torsion (HPT), asymmetric rolling (ASR) and cold rolling (CR) were adopted to introduce high, middle and low amount of strains to Al-Li-(Cu, Mg) alloys. After deformation, for the HPT processed alloys under high equivalent strains, the highest as-deformed hardness was obtained. Transmission electron microscopy (TEM) revealed that the grain size was refined to 210 nm, 120 nm and 150 nm, respectively. — Under severe plastic deformation condition (ε > 30), the Al—Li alloy lost age-hardenability, however, the aging of the asymmetric rolled Al—Li alloys increased the hardness further and the highest hardness was obtained in this alloy. For the Al-Li-Cu and Al-Li-Mg alloys, a further increase in hardness was achieved by aging the as-deformed alloys, regardless of the equivalent strains. Meanwhile, the peak hardness increases with increasing the equivalent strains. During aging treatment, the behavior of the precipitates was discussed in the present work.

1. Introduction

Aluminum-Lithium alloys are attractive especially for aerospace applications due to the low density and high strengths. Binary Al—Li alloys are strengthened by dispersion of fine precipitates. The precipitation sequence of the Al—Li alloys can be written as follows [1]:

* Corresponding author.
E-mail addresses: swlee@sus.u-toyama.ac.jp (S. Lee), tsuchiya@sus.u-toyama.ac.jp (T. Tsuchiya), matsuda@sus.u-toyama.ac.jp (K. Matsuda), horita@zaiko.kyushu-u.ac.jp (Z. Horita), robert.kocisko@tuke.sk (R. Kocisko), tobor.kvackaj@tuke.sk (T. Kvackaj).

https://doi.org/10.1016/j.matdes.2020.109139

SSSS → δ' (Al_3Li) → δ (AlLi). Generally, the aluminum alloys produced by industry undergo subsequent mechanical working and annealing (thermomechanical processing or TMP), in order to produce a finished or semi-finished product [2]. TMP has also been developed and researched for enhancing the mechanical and chemical properties of final product. The processing includes not only conventional processing (i. e. hot and cold rolling, extrusion) but also various types of newly developed deformation methods and heat-treating technology. For producing large-scaled sheets or plates with good mechanical properties, asymmetric rolling (ASR) has been proposed [3]. In ASR, the peripheral speeds of the two rolls at the contact surface are different, consequently the material is exposed to an extra shear deformation in addition to the compression deformation. Under the same rolling reduction, the effective plastic strains reached by ASR are larger than those obtained by cold rolling (CR). The schematic illustration of ASR is shown in Table 1. Among severe plastic deformation (SPD) processes, High-pressure torsion (HPT) is popular because it can continuously introduce a large amount of strain into material. HPT is a powerful method for grain refinement of metallic materials, hard-to deform materials, ceramics and intermetallic materials [4–10]. The schematic illustration of HPT is shown in Table 1. Thus, in the present work, HPT and ASR were adopted to introduce high and middle equivalent strains to the alloys.

For the age-hardenable Al—Li alloys, Mg and Cu are usually added, it has been reported that Mg addition enhances the precipitation of δ' phase due to Mg lowers the solubility of Li in the α-Al solid solution and incorporates into the δ' phase itself [11]. Furthermore, the addition of Cu leads to precipitates of T_1 (Al_2CuLi) and θ' (Al_2Cu) phases. It is known that δ', T_1 and θ' precipitates are responsible for the strengthening of Al—Li alloys. Meanwhile, the combination of deformation and aging treatment can improve the mechanical properties. In previous studies, the combined processing of SPD and aging treatment for strengthening the 2091 Al—Li alloys has been achieved [12,13], however, the effect of Cu and Mg is still unclear during aging treatment under SPD condition. In this research, except the SPD process (HPT), ASR and CR are also adopted for introducing different amount of strains to Al-Li-(Cu, Mg) alloys. HPT, ASR and CR are thought as reasonable methods for introducing high, middle and low amount of strains to Al-Li-(Cu, Mg) alloys, respectively. The aim of the present work is to investigate the effect of (1) equivalent strains(deformation methods) and (2) alloying elements (Cu and Mg) on aging behavior of the Al—Li alloys.

2. Experimental

The composition of the Al—Li, Al-Li-Cu and Al-Li-Mg alloys are shown in Table 2. The three alloys were prepared by laboratory casting and as-cast billets were homogenized at 808 K for 43.2ks, all the samples before deformation were solution treated at 833 K for 1 h and quenched in water. Deformation and heat treatment conditions are shown in Table 3.

ASR was carried out using different roll diameters with the ratio of 2.4, Samples with a dimension of 60 × 20 × 6 mm was rolled several times to about 60% thick reduction at room temperature, approximately reduction in thickness of 10% was given to the sample through every pass. The thickness of the Al—Li alloy was reduced from 6 mm to 2.2 mm after six passes, for the Al-Li-Cu and Al-Li-Mg alloy, the thickness of the sheet was reduced from 6 mm to 2.65 and 2.45 mm respectively. As shown in Table 3, the ASR was stopped at different thickness reduction in order to avoid cracks. For the Al-Li-Cu-Mg alloy, the samples broken during the ASR experiments. The ε was calculated using the follow Eq. (1) [14,15]:

Table 1
Schematic illustrations of deformation methods.

Cold rolling (CR)	Asymmetric rolling (ASR)	High-pressure torsion (HPT)
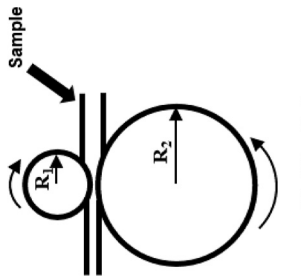		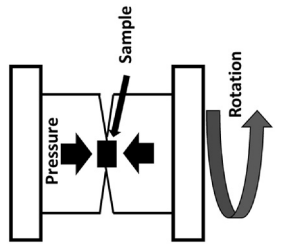
$R_2/R_1=1$	$R_2/R_1=2.4$	$R_2/R_1=2.4$
$R_2/R_1=1$	$R_2/R_1=2.4$	Eq. (1)
$\varepsilon = -\frac{2}{\sqrt{3}} \ln \frac{h}{h_0}$		$\varepsilon = \frac{2\pi r N}{\sqrt{3}h}$

Table 2
Chemical composition of used alloys.

		Li	Cu	Mg	Al
Al-Li	mol%	9.7	–	–	bal.
	wt.%	2.7	–	–	bal.
Al-Li-Cu	mol%	9.2	0.8	–	bal.
	wt.%	2.5	2.0	–	bal.
Al-Li-Mg	mol%	9.7	–	2.0	bal.
	wt.%	2.7	–	1.9	bal.

Table 3
Deformation and heat treatment conditions.

Samples	Solution treatment	Deformation	Aging temperature
Al-2.7Li		CR: 10%,30%,60% ASR: 63%,80% HPT: 5 turns	
Al-2.7Li-1.9Mg	833 K 3.6ks Water quenched	CR: 10%,30%,60% ASR: 60%,72% HPT: 5 turns	CR/ASR: 473 K HPT:423 K
Al-2.5Li-2Cu		CR: 10%,30%,60% ASR:55% HPT: 5 turns	

$$\varepsilon = \frac{\sqrt{2}}{3}\left[6\left[\ \ln 1 - \frac{h_i - h_f}{h_i}\right]^2 + \frac{6}{h_i + h_f{}^2} \times \left[R_1\ \cos^{-1}\left(\frac{2R_1 - h_i - h_f}{2R_1}\right) - R_2\ \cos^{-1}\left(\frac{2R_2 - h_i - h_f}{2R_2}\right)\right]\right]^{2}{}^{1/2} \quad (1)$$

where h_i and h_f are the initial and final sheet thickness, R_1 and R_2 correspond to the radius of the upper and bottom roll.

For the CR, the samples were cut from the hot and cold rolled sheet with a dimension of $10 \times 8 \times 3$ mm. Then, the samples were rolled to the final thickness of 1.2 mm with total thickness reduction of 60% by a single pass.

For the HPT experiment, the as-homogenized ingot was rolled to sheet through hot and cold rolling processes, then the samples for HPT were cut from the sheet in the form of disks 10 mm in diameter and 1 mm thick. The disc samples were processed for $N = 5$ turns with a rotation speed of 1.0 rpm at room temperature under a selected pressure of 6 GPa. The ε is calculated using the follow Eq. (2):

$$\varepsilon = \frac{2\pi r N}{\sqrt{3}h} \quad (2)$$

where r is the distance from the disk center, N is the number of rotations and h is the thickness of disk after HPT processing.

The aging treatment and TEM observation samples of HPT processed alloys were made along radial directions from the disc center toward the edge in the range of 2-4 mm. As shown in Table 1, the aging temperature for the as-quenched, cold rolled and asymmetric rolled samples was 473 K, however, for the HPT processed samples, the aging temperature was 423 K, as can be seen in Fig. 1, The increment of the hardness decreased with increasing the aging temperature, when the samples were aged at 343 K, although a higher increment of the hardness can be obtained, it takes a long time to reach the peak condition(for example, 277 days for the Al-Li-Mg alloy), in order to get higher age-hardenability, 423 K was chosen to age the HPT processed samples.

Microhardness of HPT and CR processed samples was measured using a hardness tester (Mitutoyo HM-101, load:100 g, duration time:15 s). The hardness measurements of HPT samples were made along radial directions from the disc center toward the edge in the range of 2-4 mm. Hardness of the ASR processed samples were taken with microhardness tester (Struers, Duramin 5, load: 200 g, duration time:15 s) on the RD-ND plane. Microstructure of samples was observed using a TOPCON EM-002B operated at 120 kV. The TEM samples were prepared by twin-jet electropolishing in a solution of 33% HNO_3 and 67% methanol at −20 °C, using a Tenupol-5 machine operating at 12 V.

3. Results

3.1. Micro Vickers hardness measurements after deformation

Fig. 2 shows the hardness of the three alloys processed by different deformation methods. It can be seen that the as-quenched hardness of the Mg and Cu added alloys was higher than that of Al—Li alloy. The as-deformed hardness of all alloys increased with increasing the ε and finally saturated to the steady state at large strains where the hardness remained unchanged with further straining. Addition of alloying element also increased the hardness under the same ε, Al-Li-Cu alloy showed the highest hardness among alloys. As shown in Fig. 2, under the same thickness reduction, the ε introduced by ASR is higher than CR, and the ASR samples showed higher as-deformed hardness level than the CR samples, i. e., the hardness of the Al-Li-Mg alloy after ASR was about 125 HV, while the hardness after CR was about 103 HV. Compared to ASR and CR, HPT significantly increased the hardness after deformation, in particular, for the alloys with addition of Cu or Mg.

3.2. Aging behavior of Al-Li-(Cu, Mg) alloys

Fig. 3 shows the age hardening behavior of the three alloys with and without deformations. The aging temperature for the undeformed, ASR and CR samples was 473 K and for the HPT sample was 423 K. In Fig. 3 (a), the as-HPT sample showed a high initial hardness value(127 HV), however, aging at 423 K decreased the hardness. For the ASR and CR samples, there was a significant increase in hardness during aging.

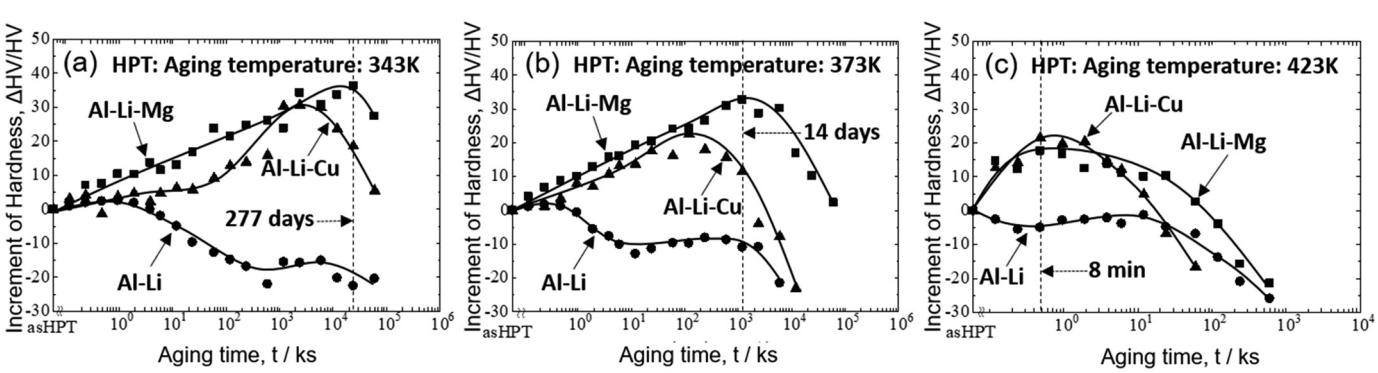

Fig. 1. Aging hardening abilities of the HPT processed Al—Li, Al-Li-Mg and Al-Li-Cu alloys aged at 343 K, 373 K and 423 K.

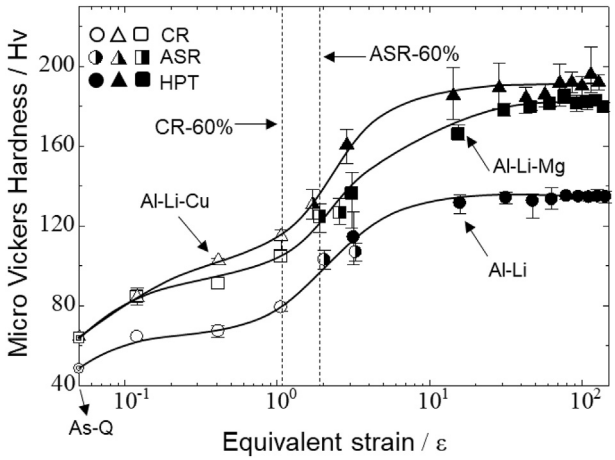

Fig. 2. Micro Vickers hardness as a function of the equivalent strain (ε) in the CR, ASR and HPT processed samples.

The peak hardness value of the ASR samples was 140 HV, which was higher than that of the peak-aged sample without deformation (117 HV) and samples processed by HPT. It is noteworthy that the ASR sample exhibited the highest peak hardness in the Al—Li binary alloy. As shown in Fig. 3(b), the peak hardness of the Al-Li-Mg alloy reached almost the same level as that of the Al—Li alloy under the undeformed condition, hardness of all the deformed Al-Li-Mg samples can be increased by aging treatment and the peak-hardness increased with increasing the ε. Addition of Mg not only increased the as-deformed hardness but also made the HPT processed samples obtained age-hardenability. The aging behavior of the Al-Li-Cu alloy was shown in Fig. 3(c), with the addition of Cu, the peak-hardness of the undeformed samples was higher than the undeformed Al—Li and Al-Li-Mg alloys. Different to the Al-Li-Mg alloy, there was a small difference between the peak hardness of the ASR and CR samples in Al-Li-Cu alloy. For all alloys, the peak hardness of the deformed samples was higher than that without deformation, regardless of the alloy composition. Also, the peak hardness occurred earlier in the deformed samples. In contrast to the Al—Li alloy, the highest peak-aged hardness for Al-Li-Mg and Al-Li-Cu alloys was obtained by HPT and subsequent aging treatment.

Fig. 4 shows the age-hardenability of the alloys with and without deformations, the age-hardenability was evaluated by the increment of the hardness, as can be seen, the as-quenched alloys possessed the largest age-hardenability in all the alloys. However, as shown in Fig. 4 (a) and (c), before 3.84ks, the age-hardening rate in CR processed Al—Li and Al-Li-Cu alloys was higher than that after quenching. Although high values of hardness were achieved by HPT processing, the age-hardenability of the HPT processed alloys was the lowest.

3.3. TEM microstructure observation of samples without deformation

Fig. 5 shows TEM bright field (BF) and dark field (DF) images of the as-quenched and peak-aged samples. It can be found that relatively small δ' phase formed in the matrix of all the alloys during quenching or immediately after quenching, as shown in Fig. 5(a), (e) and (i). The metastable δ' phase has an $L1_2$ superlattice crystal structure and is coherent with the matrix [1]. Previous investigations have shown that the δ' phase already precipitates in the as-quenched stage due to the δ' phase small lattice misfit and low interfacial energy [1]. The reported

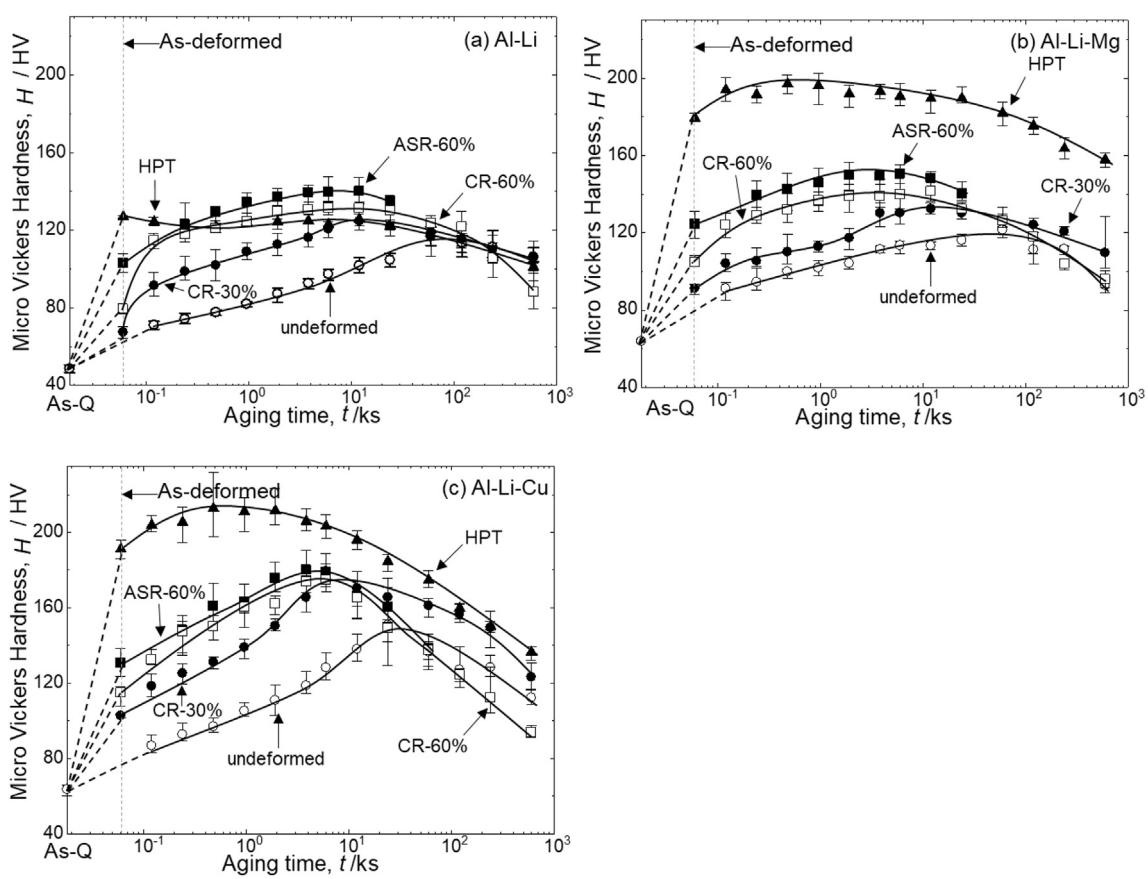

Fig. 3. Age hardening behavior of the (a) Al—Li, (b) Al-Li-Mg and Al-Li-Cu alloys with and without deformations. The aging temperature of the undeformed, CR and ASR samples was 473 K and for the HPT sample was 423 K.

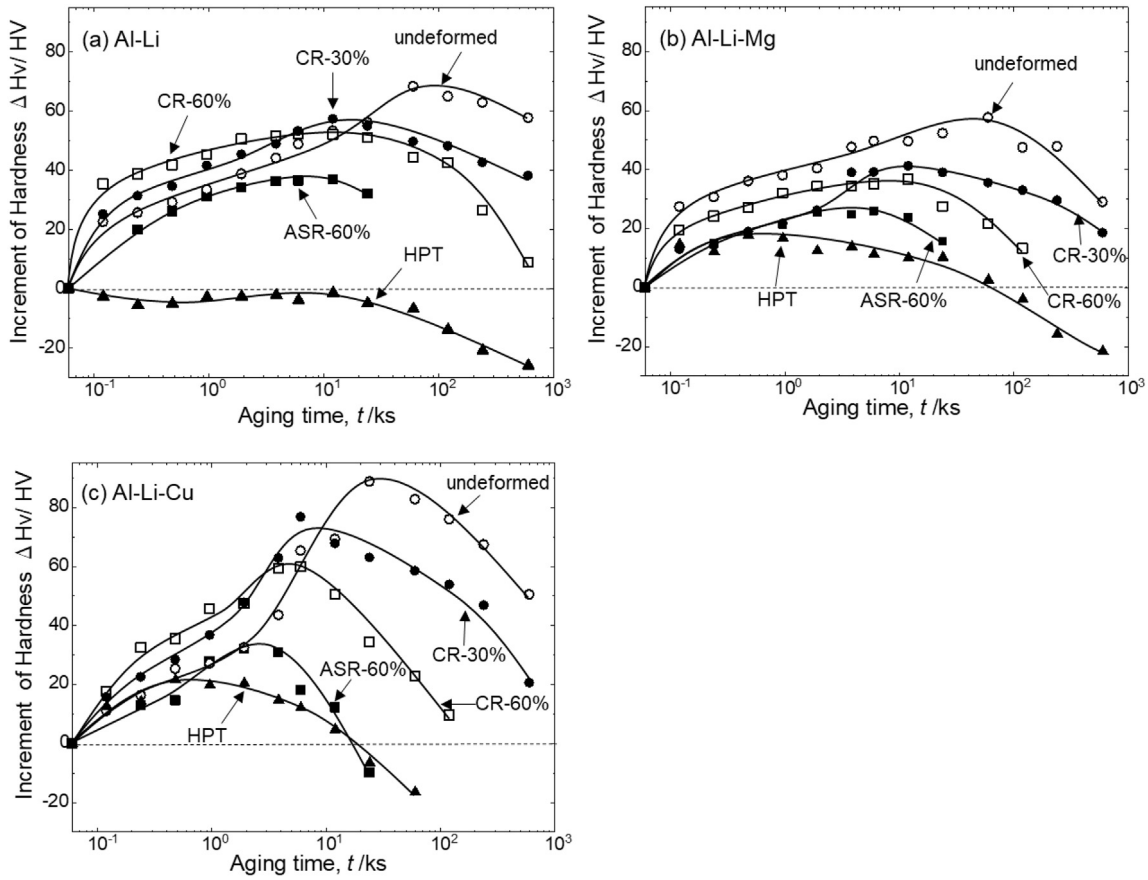

Fig. 4. Aging hardening abilities of the (a) Al—Li, (b) Al-Li-Mg and Al-Li-Cu alloys with and without deformations.

behaviors are in agreement with the results obtained here for the three alloys containing more than 2 wt%-Li. In the as-quenched state, the number density of the δ' phase was about 5400/μm^2, 7000/μm^2 and 5100/μm^2 in the Al—Li, Al-Li-Cu and Al-Li-Mg alloys, after aging treatment, the number density of the peak-aged alloys decreased to about 680/μm^2, 470/μm^2 and 600/μm^2, respectively.

As shown in Fig. 5(c), (g) and (k), the spherical δ' phase was observed in all the peak-aged alloys. The average size of the δ' phase in the Al—Li and Al-Li-Cu alloys was about 28 nm. With the addition of Mg, the size of the δ' phase increased to about 31 nm under the peak-aged condition. In addition, T_1 (Al_2CuLi) and θ' (Al_2Cu) phases also precipitated from the matrix of Al-Li-Cu alloy during aging. The θ' precipitates are rarely observed, in which the δ' and T_1 phase were the two main strengthening precipitates types. For the Al-Li-Mg alloy, the stable S_1 (Al_2MgLi) phase [16,17] was occasionally found in the peak-aged condition, as marked with arrow in Fig. 5(j). From the dark field image, Fig. 5(k), it is clear that the S_1 phase was surrounded by δ'-precipitate-free zones (PFZ).

3.4. Microstructure of the deformed alloys

3.4.1. TEM microstructure of the as-deformed alloys

The as-deformed microstructure of the HPT and ASR samples is shown in Fig. 6. As seen from Fig. 6(a)-(c), equiaxed ultrafine grains formed during HPT process. The average grain size of the Al—Li, Al-Li-Mg and Al-Li-Cu alloy was about 210 nm, 150 nm and 120 nm, respectively. Thus, the addition of Mg or Cu promoted the formation of a finer grain structure during HPT process. Fig. 6(d)-(f) shows the microstructure after the ASR. Due to the introduced equivalent strain by ASR is lower than HPT, it is not shown the fully recrystallized structure like the HPT processed microstructure. It is possible to observe some subgrains and dislocation cell (or tangled dislocation).

Fig. 7 shows the selected area electron diffraction (SAED) patterns of the three alloys after deformations. Based on Fig. 7(a), (b) and (c), most of these grains in ASR processed alloys were separated by low-angle boundaries due to the ASR introduced ε was low. However, the SAED pattern of the HPT processed Al—Li alloy in Fig. 7(d) exhibited rings indicative of grains separated by boundaries having high angles of misorientation. Also, the δ' phase can be detected from all the deformed samples, it means that δ' phase existed in the as-deformed alloys.

3.4.2. TEM microstructure of peak-aged condition

Fig. 8 shows the microstructures of the three alloys after deformation and subsequent aging treatment. The dark filed images revealed that, under the peak-aged condition, the average size of the δ' phase decreased with increasing the ε. Obvious growth of the δ' phase was confirmed in the CR processed alloys because of the prolonged aging time. As shown in Fig. 8(a), (c) and (d), (f), under the same aging condition, the average sizes of the δ' phase in the Al-Li-Mg alloy processed by CR are also larger than that in Al—Li alloy. At the same time, the larger δ' phase is visible along the dislocations. The average size of the δ' phase will be discussed later.

For the peak-aged Al-Li-Cu alloy, T_1 phase formed in the CR and ASR samples, as shown in Fig. 8(b) and (e), severe interactions of the T_1 with the δ' could be easily identified. In the ASR sample, except the finer T_1 phase in the grain interior, the coarsening of the T_1 precipitates adjacent to low angle grain boundaries (LAGBs) during aging was also found, as shown in Fig. 8(h).

The HPT processed samples are shown in Fig. 9. As seen in Fig. 9(a)-(f), the δ' can be detected in the grains of the as-HPT samples. Because of

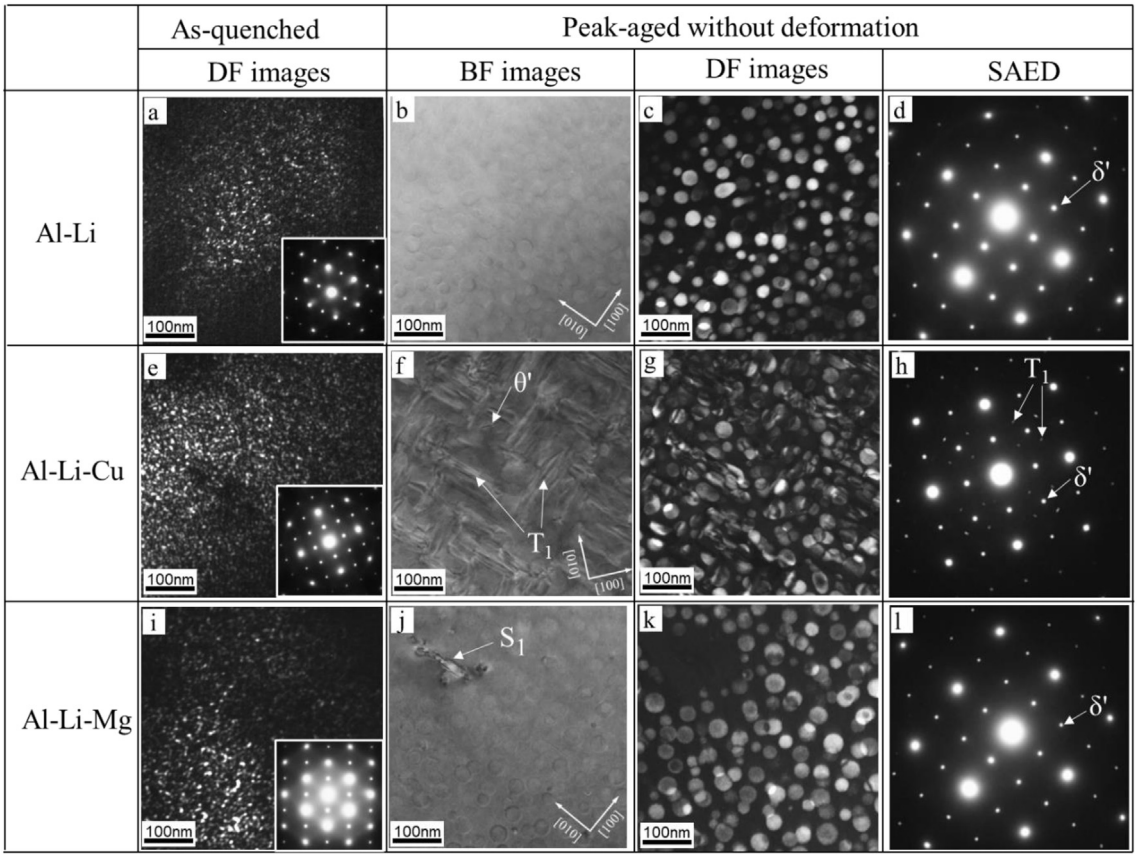

Fig. 5. TEM images of the as-quenched and peak-aged samples of (a-d) Al—Li, (e-h) Al-Li-Cu and (i-l) Al-Li-Mg alloys. Aging condition for the Al—Li and Al-Li-Cu alloys was 473 K/60ks, for the Al-Li-Cu was 473 K/24ks.

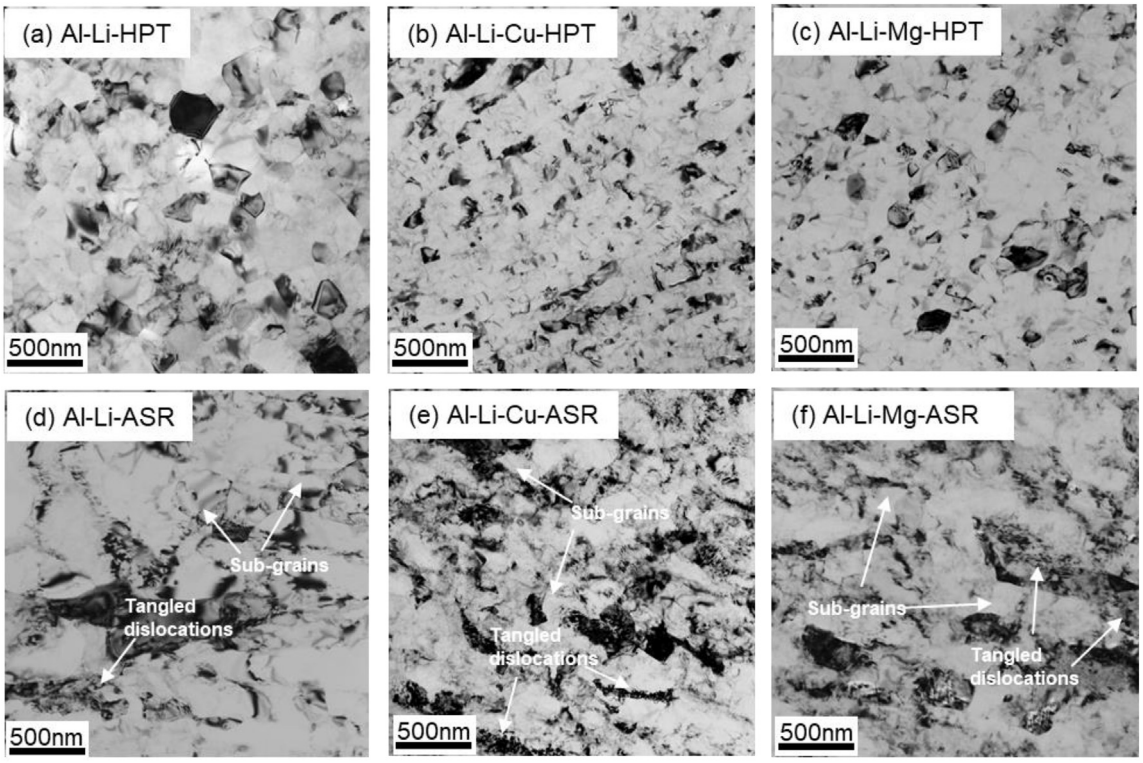

Fig. 6. TEM micrographs of the Al—Li, Al-Li-Cu and Al-Li-Mg alloys processed by (a-c) HPT and (d-f) ASR.

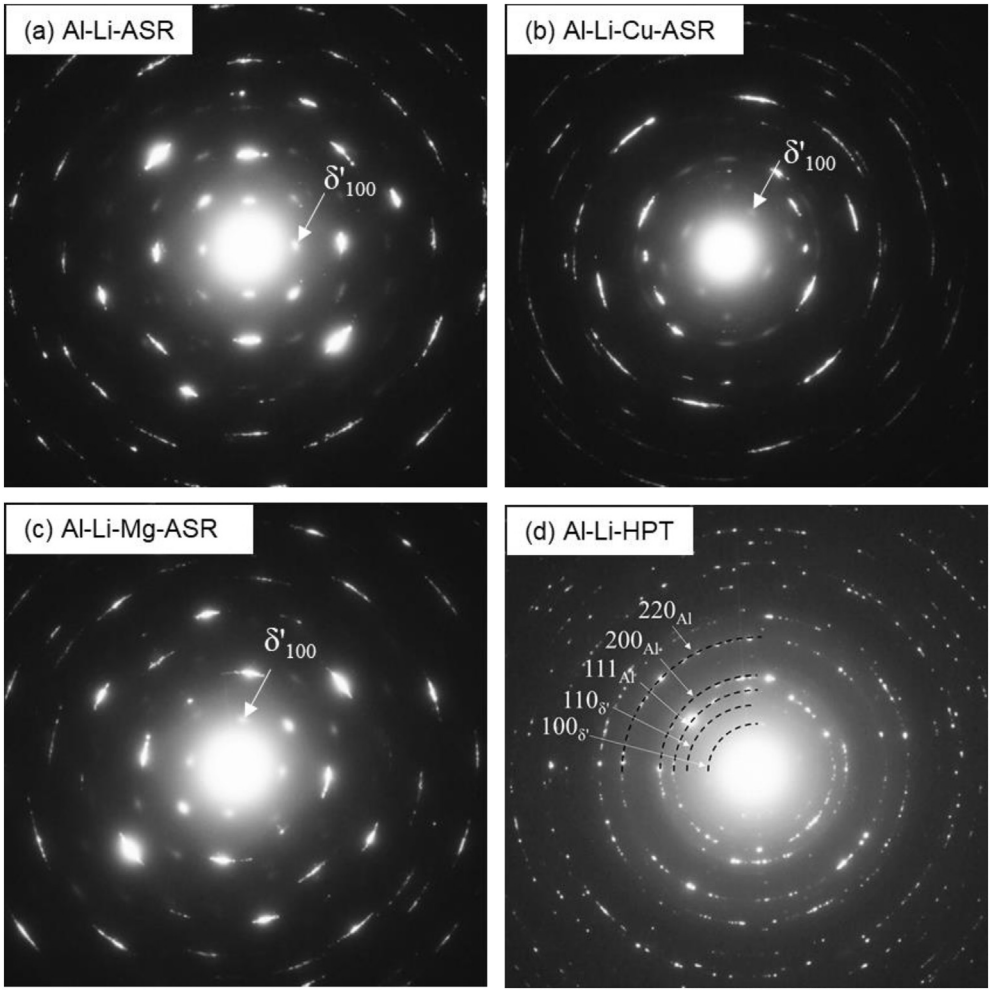

Fig. 7. SAED patterns of the ASR processed (a)Al-Li, (b) Al-Li-Cu, (c) Al-Li-Mg alloys and (d) HPT processed Al—Li alloy. (a), (b), (c) and (d) is the corresponding SAED patterns of Fig. 5 (d), (e), (f) and (a).

the irregular morphology, the size of the δ' phase in the as-HPT sample is not given here. As shown in Fig. 9(h), T_1 phase was not detected in the grain interior of the peak-aged HPT sample of Al-Li-Cu. This suggests that only δ' phase contributed to increase the hardness in the Al-Li-Cu and Al-Li-Mg alloys.

Fig. 10 shows the microstructure of the three alloys under over-aged condition. When the aging time increased to 60ks, obvious growth of the δ' phase can be observed in the grains as compared to the peak-aged samples. As seen in Fig. 10(g)-(i), the precipitate formed within grain interiors was only δ' phase in the Al—Li and Al-Li-Mg alloys. For the Al-Li-Cu alloy, as shown in Fig. 10(b) and (h), the T_1 phase was detected in the grains. With the addition of Mg, as shown in Fig. 10(f), the S_1 phase is found at the grain boundaries and a PFZ zones of δ' phase formed around the S_1 phase, The larger size of the δ' phase near the PFZ zones due to a lower nucleation density adjacent to the PFZ such that fewer precipitates form and subsequently grow to a larger size during aging. Alternatively, the precipitates bordering the PFZ may draw solute from within the PFZ and grow larger compared to the precipitates deeper within the grains [18].

3.5. Grain growth of the deformed alloys

Fig. 11 shows the grain size as function of aging time. In case of the HPT samples, when the aging time was 0.48ks, the average grain size of the Al—Li alloy increased slightly, however, the Cu and Mg added alloys was unchanged. For the Al—Li alloy, the average grain size increased from about 210 nm to 400 nm after aging at 423 K for 600ks. Under the same aging condition, the average grain size of the Al-Li-Cu and Al-Li-Mg alloys only increased to about 210 nm and 220 nm, respectively. It suggested that the grain growth of the Al-Li-Cu and Al-Li-Mg alloys was suppressed. As shown in the Fig. 11, recrystallized grains and dislocation cell sizes of the Cu and Mg added alloys are also smaller than the Al—Li alloy.

4. Discussion

4.1. Effect of alloying element

4.1.1. Solution treated condition

With the addition of Cu and Mg, the as-quenched hardness increased. The solid solution strengthening can be roughly estimated by using the formula as follow [19,20]:

$$\delta_{ss}^{X} = A_X C_X^{2/3} \tag{3}$$

where δ_{ss}^{X} is the strength increment contributed from solute atoms X, A_X is the constant and C_X is the concentration of the solute in weight percent. The A_X values for Li, Cu and Mg atoms are: $A_{Li} = 10.862$, $A_{Cu} = 12.132$, $A_{Mg} = 20.481$, the C_X for the studied alloys is listed in Table 2. According to Eq. (3) and by using Taylor factor of 3, the converted hardness was estimated to be 6.7, 13.1 and 17.5 HV for the Al—Li, Al-Li-Cu and Al-Li-Mg alloys, respectively. In addition, the hardness of the annealed pure Al is about 20 [21]. Thus, the calculated hardness of

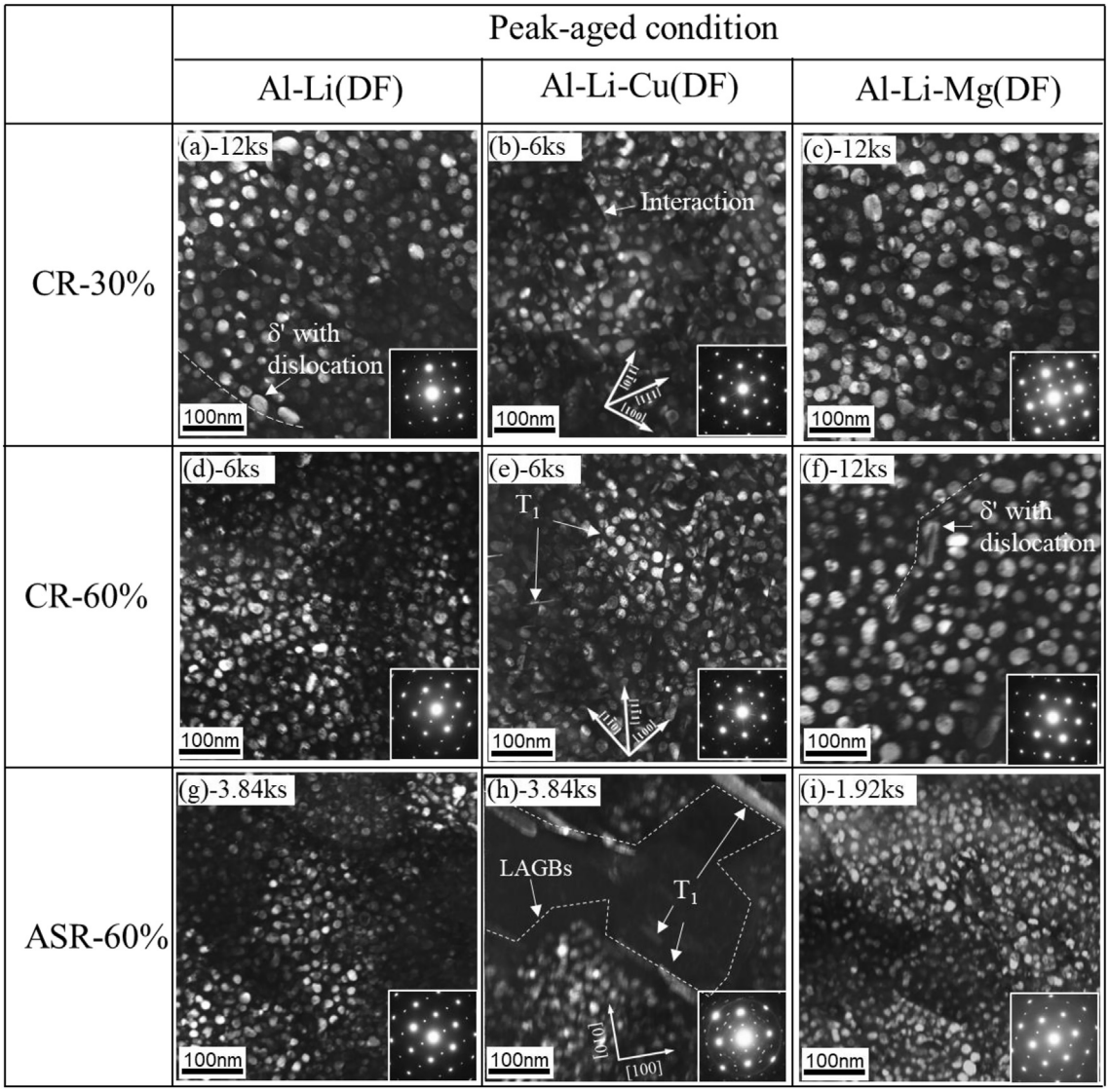

Fig. 8. TEM dark filed images of the peak-aged samples. The corresponding SAED patterns were shown in the insets in the lower right. Aging temperature for all the samples was 473 K.

the studied Al—Li, Al-Li-Cu and Al-Li-Mg alloys was 26.7 HV, 33.1 HV and 37.5 HV, respectively. However, the fine δ' phase forms in the as-quenched condition and results in the hardness increase after quenching, as shown in Table 5, the measured hardness of the Al—Li alloy was 48 HV, obviously, the measured hardness after quenching was higher than the calculation (26.7 HV). Therefore, a hardness increase of about ΔHV21, ΔHV30 and ΔHV27 was achieved in the Al—Li, Al-Li-Cu and Al-Li-Mg alloys, respectively, due to the formation of fine δ' phase in the as-quenched state.

4.1.2. After deformation

Ultrafine grains with high angle boundaries formed after HPT as a result of the high ε introduced. As seen in Fig. 6, the average grain size of Al—Li alloys is 210 nm, addition of Cu and Mg enhanced the HPT induced refinement of the microstructure of Al—Li alloy. Cu addition is more effective than Mg in refining the grain size. The average grain size of the Al-Li-Cu and Al-Li-Mg alloy is 120 nm and 150 nm, respectively. The fine grain refinement with the addition of Cu or Mg is owing to the effect of atomic-size and modulus mismatch on the mobility of the dislocations [22]. The presence of Mg or Cu atoms increases the localized stress needed for dislocation motion, thus reduce the dislocation recovery, dynamic recrystallization and grain boundary migration during HPT processing. Cu is more effective than Mg in inhibiting dynamic recovery [23]. This also explains why the Al-Li-Cu alloys always exhibit the highest hardness under different ε. Recently, many studies have confirmed the deformation induced solute segregation at grain boundaries [24–28], for instance, Xu found that Cu atoms segregate at grain boundaries during plastic deformation due to dynamic interaction between Cu atoms with gliding dislocations, segregation of Cu atoms at grain boundaries play a crucial role in stabilizing the nanostructures [24]. Segregation of Mg has also been investigated in Al—Mg alloys [27,28], it shows that the HPT processed Al—Mg alloys exhibit higher strength than the Hall-petch relationship predicts, the enhanced strength is attributed to segregation of Mg at the grain boundaries, it is concluded that the addition of Mg can amplify the Hall-Petch type GB strengthening. Thus, the Cu and Mg addition influences SPD-processed materials not only through a more enhanced grain refinement but also through grain boundary segregation of Cu and Mg atoms.

For the ASR samples, recrystallized grains and dislocation cell size of the Cu and Mg added alloys was also smaller than the Al—Li alloy. These boundaries are less effectively in promoting grain boundary strengthening, because low angle boundaries are weaker obstacles for dislocation movements [29].

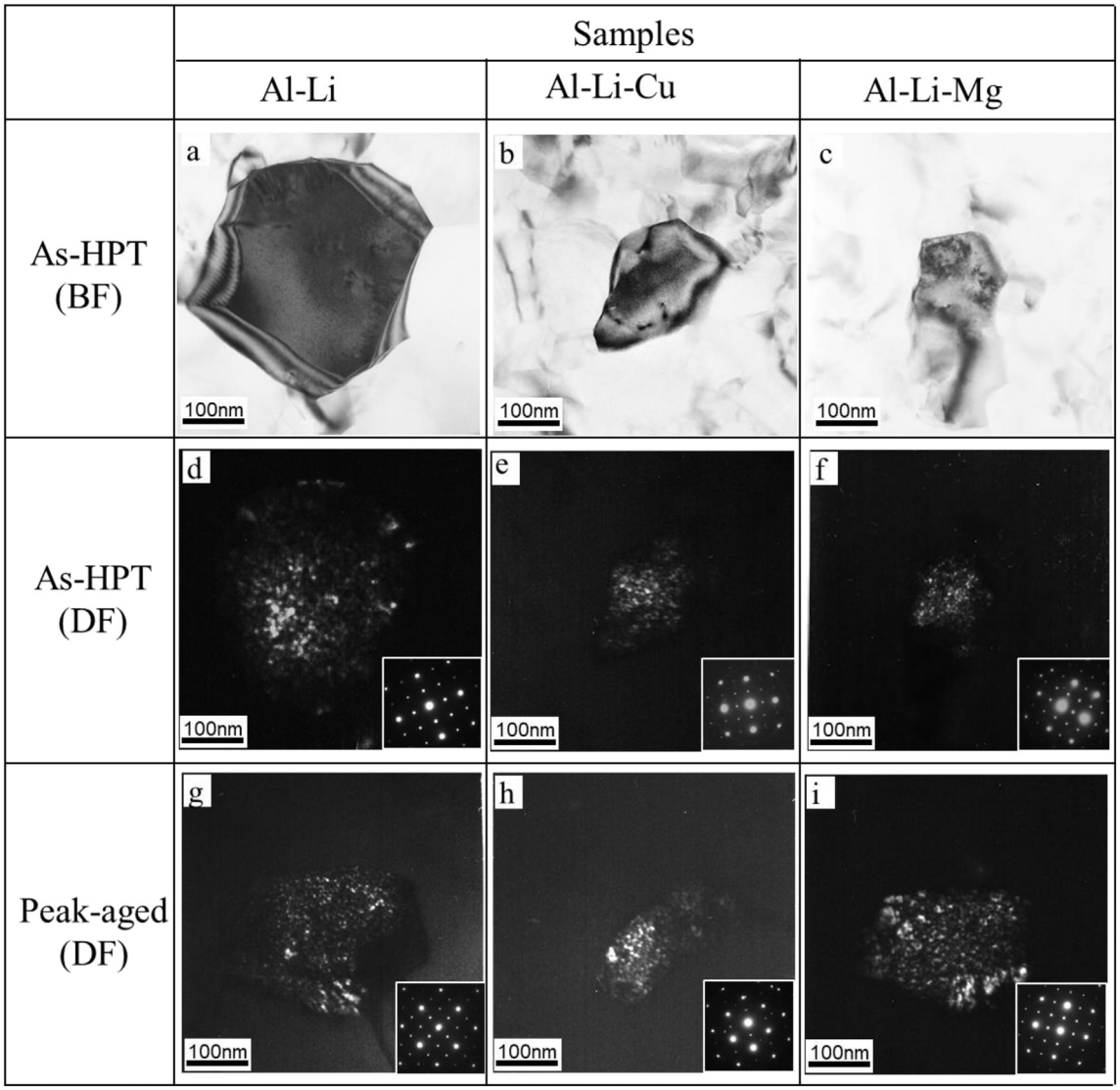

Fig. 9. TEM bright field and dark filed images of the three alloys after (a-f) HPT and (g-i) HPT and aged at 423 K for 0.48ks. The corresponding SAED patterns were shown in the insets in the lower right of the dark filed images.

4.1.3. Aging behavior

In comparison to the Al—Li alloy, the average size of the δ' phase in Al-Li-Mg alloys was always larger than the Al—Li alloy from as-quenched state, as shown in Table 4. However, the number density of the Al-Li-Mg alloy was lower, it suggested that Mg addition increases the average size of the δ' phase from as-quenched state as compared to binary Al—Li alloy. In spite of the initial hardness of Mg added alloy was higher than the Al—Li alloy, the two alloys exhibited a similar peak hardness when aged at 473 K, as seen in Fig. 3. These results indicated that the precipitation of the incoherent S_1 phase combined with the formation of δ'-PFZs leads to material softening in the Al-Li-Mg alloy. With the addition of Cu, except the δ' phase, the T_1 and θ' phase also formed in the matrix, especially the T_1 phase, which orientation relationship with the matrix is $\{0001\}_{T1}//\{111\}_{Al}$ and $\langle 1010\rangle_{T1}//\langle 110\rangle_{Al}$ [30]. It impedes the dislocation glide along the $\{111\}_{Al}$ plane and therefore contribute more to strengthening than precipitates like δ' and θ' phase [31]. This is the reason that the ΔHV of the Al-Li-Cu alloy was higher than the Al—Li and Al-Li-Mg alloys.

As seen in Table 4, with increasing the ε, the average size of the δ' phase decreased under the peak-aged condition. For the Al—Li and Al-Li-Mg alloys after CR and ASR, the hardness increase of the Al—Li and Al-Li-Mg alloys resulted from the precipitation and growth of δ' phase. As shown in Fig. 4(a), the CR processed samples exhibited a higher initial age-hardening rate than the as-quenched samples, indicating that the presence of dislocations facilitated the growth of δ' phase [32]. When the $\varepsilon < 2$, the age-hardenability of the Al—Li alloy was always higher than the Al-Li-Mg alloy, however, under the SPD condition ($\varepsilon > 30$), the Al—Li alloy lost the age-hardenability, even the alloy was aged at 343 K, the highest hardness increment was only 2.6 HV, as shown in Fig. 1. The similar results were also reported in the reference [33], the Al-0.7wt%Li and Al-1.6wt%Li alloys were processed by hydrostatic extrusion(HE) and equal channel angular extrusion(ECAP), even the as-deformed alloys annealed at the lowest temperature (373 K), the hardness decreased due to recovery. As shown in Fig. 11, compare to Al-Li-Cu and Al-Li-Mg alloys, there was a small increase in the average grain size of the Al—Li alloy when aged at 423 K for 0.48ks. Apparently, the precipitation and growth of δ' phase cannot compensate the reduced grain boundary and dislocation strengthening in the Al—Li alloy. The grain growth of the HPT processed Cu and Mg added alloys was suppressed during aging. It is well known that the presence of solute or impurity segregation in grain boundary regions imposes a drag force on the GB and reduces the driven force for grain

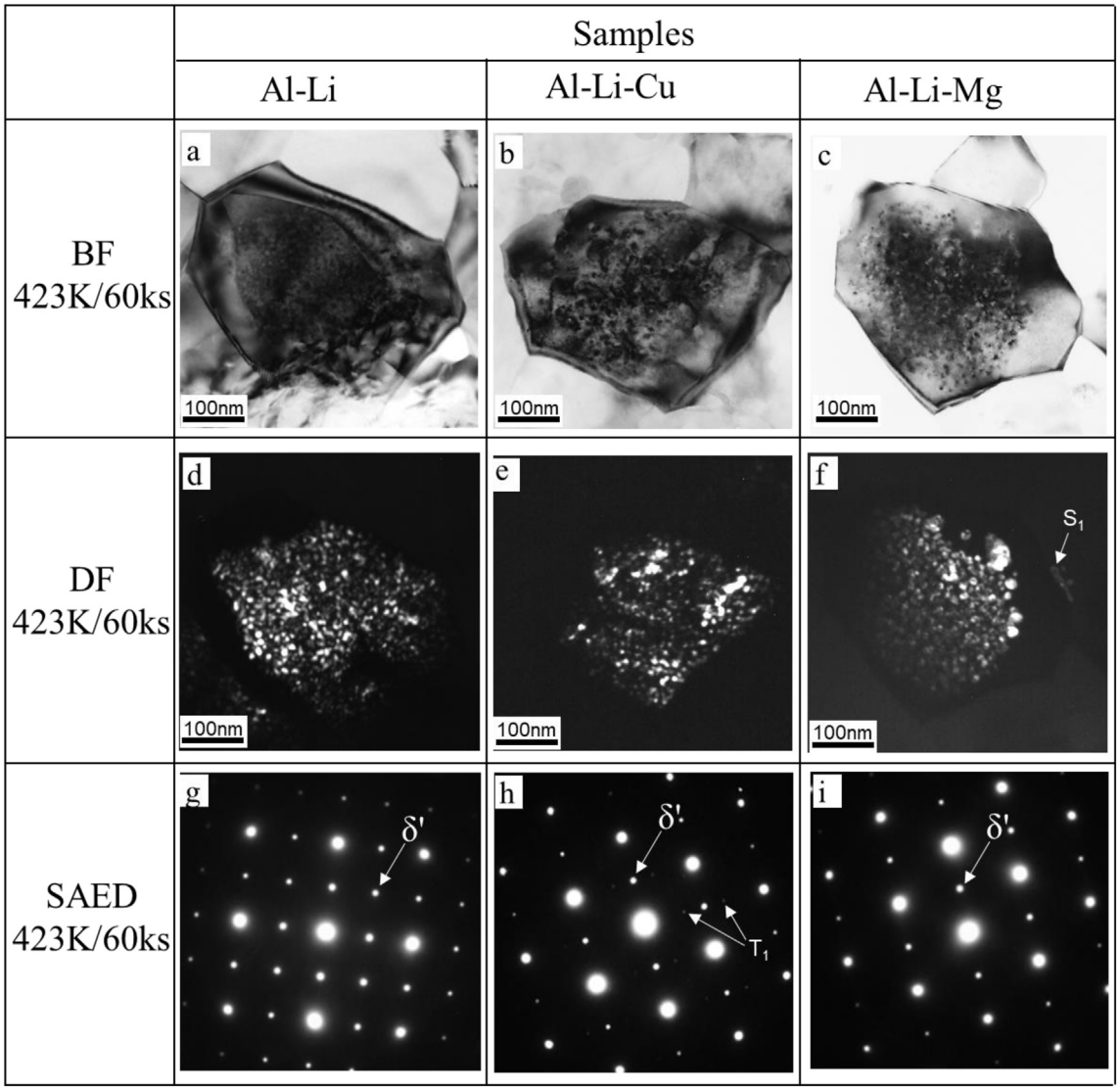

Fig. 10. TEM bright field, dark filed images and SAED patterns of the three alloys after HPT and aged at 423 K for 60ks (over-aged condition). The SAED patterns were taken from the grain interior.

growth due to the decrease in grain boundary energy [34,35]. The precipitates formed at the grain boundaries during aging can also pin the grain boundaries. Therefore, the grain growth rate of the Cu and Mg added alloys is suppressed. Although the hardness of the HPT processed Al—Li alloy decreased upon aging, with the addition of Cu and Mg, the hardness of the HPT processed samples increased and reached the peak rapidly(0.48ks). As shown in Fig. 9, the T_1 phase was not found in the grain interior of the peak-aged HPT processed Al-Li-Cu alloy, there is no doubt that the precipitation and growth of δ' phase contributes to the hardness during aging. In addition, the annealing(aging) induced hardening has been confirmed in Al—Cu and Al—Mg alloys after

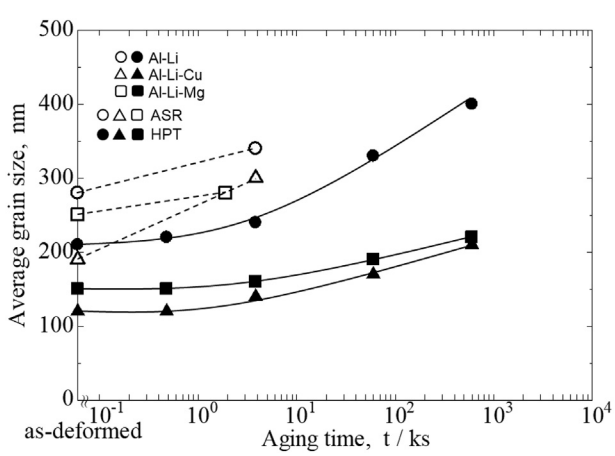

Fig. 11. The grain size of the HPT and ASR processed Al-Li-(Mg, Cu) alloys during aging treatment.

Table 4
The average size of δ' phase.

	δ' size (nm)				
	Without deformation		CR/60%	ASR	HPT
	As-Q	Peak-aged	Peak-aged	Peak-aged	Peak-aged
Al-Li	~4.6	~28	~17	~12	~4.5
Al-Li-Cu	~4.6	~28	~18	~14	~4.6
Al-Li-Mg	~5.4	~31	~22	~12	~4.5

Table 5
Summary of hardness variations (HV).

	Without deformation			CR			ASR			HPT		
	As-Q	Peak-aged	ΔHV	As-CR	Peak-aged	ΔHV	As-ASR	Peak-aged	ΔHV	As-HPT	Peak-aged	ΔHV
				10 / 30 / 60%	10 / 30 / 60%	10 / 30 / 60%						
Al-Li	48	117	69	65/67/79	119/125/131	54/60/52	103	140	37	127	127	0
Al-Li-Cu	63	151	88	84/103/115	163/179/175	79/76/60	131	180	49	191	213	22
Al-Li-Mg	64	121	57	85/91/105	125/132/141	40/41/36	125	150	25	179	197	18

SPD [36,37], it was shown that the hardening of ECAP processed Al-5wt %Cu alloy was due to aging-induced relaxation of non-equilibrium HAGBs with enhanced grain boundary segregations of Cu. In the present work, this may also contribute to increase the hardness in the initial stage of aging.

Above all, through combination of deformation and aging treatment, hardness of all the alloys were improved except HPT processed Al—Li alloy. It is suggested that concurrent strengthening by grain refinement and precipitation hardening is hardly activated in the binary Al—Li alloy. Severe plastic deformation will make the binary Al—Li alloy lose age-hardenability, the combination of ASR with medium ε and aging treatment is better for strengthening the binary Al—Li alloy. However, according to Fig. 3, with the addition of Mg or Cu, since the peak-aged hardness increases with increasing the ε before reaching the stead-state, a highly introduced ε is helpful to strengthen the alloys. Moreover, for the Al-Li-Cu alloy, a lowly introduced ε effectively increased the peak-hardness as compare to the Al-Li-Mg alloy, due to dislocation enhances the precipitation of T_1 phase [38], however, in the case of ASR, the hardness increase between ASR and CR samples was smaller than that in Al-Li-Mg alloy. As shown in Fig. 8(h), T_1 phase coarsened at the low angle boundaries, this suggests that the introduced ε during deformation should avoid forming low angle boundaries, coarsening of T_1 phase along the low angle boundaries may affect the properties of Al-Li-Cu alloy [39,40].

5. Conclusion

1. With addition of Mg or Cu, microhardness of the Al—Li alloys increased after deformation. Cu is more effective than Mg for improving the as-deformed hardness under different ε.
2. In the case of the ASR, the microstructure after deformation formed the dislocation cell (or tangled dislocation) and recrystallized grains. After processed by HPT, an ultrafine-grained structure with a grain size of 210 nm, 120 nm and 150 nm was achieved in the Al—Li, Al-Li-Cu and Al-Li-Mg alloys, respectively. Addition of Cu or Mg enhances grain refinement and suppresses grain growth of the ultrafine Al—Li alloy during aging treatment.
3. With different amount of introduced ε, aging times for reaching peak aging are different. Higher ε causes shorter time for reaching peak aging. For the binary Al—Li alloy, severe plastic deformation ($\varepsilon > 30$) made it lose age-hardenability, however, the aging of asymmetric rolled Al—Li alloys increased the hardness further and the highest hardness was obtained. With the addition of Cu or Mg, the as-deformed hardness can be further increased by aging treatment, regardless of the strains. During aging treatment, the peak hardness increases with increasing the equivalent strains.
4. In the Al-Li-Mg alloy, S_1 phase appeared in the peak-aged condition of preciously non-deformed samples. In the Al-Li-Cu alloy, T_1 phase formed in the grain interior of peak-aged ASR, CR and undeformed samples. Coarsening of T_1 phase was also confirmed along the low angle boundaries in the ASR processed samples. However, T_1 phase was not found in the grain interior of peak-aged HPT samples.

Declaration of Competing Interest

The authors declare that they have no known competing financial interests or personal relationships that could have appeared to influence the work reported in this paper.

Acknowledgements

The authors would like to thank Erasmus+ Program, project nr: 2017-1-SK01-KA107-035143, Light Metal Educational Foundation (2018-2019) and President description, university of Toyama (2019). We thank Prof. Seiji Saikawa (University of Toyama) for providing casting samples. We thank Mr. Yuhei Haizuka (University of Toyama) and Mr. Yosuke Hasegawa(University of Toyama) for helping the experiments.

References

[1] B. Noble, G.E. Thompson, Precipitation characteristics of aluminium-lithium alloys, Met. Sci. J. 5 (1971) 114–120, https://doi.org/10.1179/030634571790439333.
[2] F.J. Humphreys, G.W. Lorimer, Thermomechanical processing of aluminium alloys, in: R. Ciach (Ed.), Advanced Light Alloys and Composites. NATO ASI Series (3. High Technology), vol 59, Springer, Dordrecht, 1998 https://doi.org/10.1007/978-94-015-9068-6_44.
[3] S.A.E. Buxton, S.C. Browning, Turn-Up and turn-down in hot rolling: A study on a model mill using plasticine, J. Mech. Eng. Sci. 14 (1972) 245–254, https://doi.org/10.1243/JMES_JOUR_1972_014_032_02.
[4] I.V. Shchetinin, I.G. Bordyuzhin, R.V. Sundeev, V.P. Menushenkov, A.V. Kamynin, V.N. Verbetsky, A.G. Savchenko, Structure and magnetic properties of $Sm_2Fe_{17}Nx$ alloys after severe plastic deformation by high pressure torsion, Mater. Lett. 274 (2020) 127993, https://doi.org/10.1016/j.matlet.2020.127993.
[5] S. Lee, K. Edalati, Z. Horita, Microstructures and mechanical properties of Pure V and Mo processed by high-pressure torsion, Mater. Trans. 51 (2010) 1072–1079, https://doi.org/10.2320/matertrans.M2009375.
[6] S. Lee, Z. Horita, High-pressure torsion for pure chromium and niobium, Mater. Trans. 53 (2012) 38–45, https://doi.org/10.2320/matertrans.MD201131.
[7] D.V. Gunderov, A.A. Churakova, V.V. Astanin, R.N. Asfandiyarov, H. Hahn, R.Z. Valiev, Accumulative HPT of Zr-based bulk metallic glasses, Mater. Lett. 261 (2020) 127000, https://doi.org/10.1016/j.matlet.2019.127000.
[8] J. Gubicza, P. Hung, M. Kawasaki, J. Han, Y. Zhao, Y. Xue, J. Lábár, Influence of severe plastic deformation on the microstructure and hardness of a CoCrFeNi high-entropy alloy: A comparison with CoCrFeNiMn, Mater. Charact. 154 (2019) 304–314, https://doi.org/10.1016/j.matchar.2019.06.015.
[9] K. Edalati, Z. Horita, Application of high-pressure torsion for consolidation of ceramic powders, Scr. Mater. 63 (2010) 174–177, https://doi.org/10.1016/j.scriptamat.2010.03.048.
[10] R.V. Sundeev, A.V. Shalimova, A.A. Veligzhanin, A.M. Glezer, Y.V. Zubavichus, Difference between local atomic structures of the amorphous Ti_2NiCu alloy prepared by melt quenching and severe plastic deformation, Mater. Lett. 214 (2018) 115–118 http://www.sciencedirect.com/science/article/pii/S0167577X17317354.
[11] A. Deschamps, C. Sigli, T. Mourey, F. de Geuser, W. Lefebvre, B. Davo, Experimental and modelling assessment of precipitation kinetics in an Al–Li–Mg alloy, Acta Mater. 60 (2012) 1917–1928, https://doi.org/10.1016/j.actamat.2012.01.010.
[12] S. Hirosawa, T. Hamaoka, Z. Horita, S. Lee, K. Matsuda, D. Terada, Methods for designing concurrently strengthened severely deformed Age-hardenable Aluminum alloys by ultrafine-grained and precipitation hardenings, Metall. Mater. Trans. A. 44A (2013) 3921–3933, https://doi.org/10.1007/s11661-013-1730-y.
[13] S. Lee, Z. Horita, S. Hirosawa, K. Matsuda, Age-hardening of an Al–Li–Cu–Mg alloy (2091) processed by high-pressure torsion, Mater. Sci. Eng. A 546 (2012) 82–89, https://doi.org/10.1016/j.msea.2012.03.029.
[14] S.B. Kang, B.K. Min, H.W. Kim, D.S. Wilkinson, J. Kang, Effect of asymmetric rolling on the texture and mechanical properties of AA6111-aluminum sheet, Metall. Mater. Trans. A. 36 (2005) 3141–3149, https://doi.org/10.1007/s11661-005-0085-4.

[15] J. Sidor, A. Miroux, R. Petrov, L. Kestens, Microstructural and crystallographic aspects of conventional and asymmetric rolling processes, Acta Mater. 56 (2008) 2495–2507, https://doi.org/10.1016/j.actamat.2008.01.042.
[16] S.F. Baumann, D.B. Williams, A new method for the determination of the precipitate-matrix interfacial energy, Scr. Metall. 18 (1984) 611–616, https://doi.org/10.1016/0036-9748(84)90351-X.
[17] V.G. Davydov, L.B. Ber, E. Ya, V.I. Komov Kaputkin, O.G. Ukolova, E.A. Lukina, TTP and TTT diagrams for quench sensitivity and ageing of 1424 alloy, Mater. Sci. Eng. A 280 (2000) 76–82, https://doi.org/10.1016/S0921-5093(99)00659-0.
[18] J. Song, R. Field, D. Konitzer, M. Kaufman, Development of Grain Boundary Precipitate-Free Zones in a Ni-Mo-Cr-W Alloy, Metall Mat Trans A. 48 (2017) 2425–2434, https://doi.org/10.1007/s11661-017-4019-8.
[19] G.E. Totten, D.S. MacKenzie, Handbook of Aluminum: Vol. 1 - Physical Metallurgy and Processes, CRC press, New York, 2003.
[20] Z.X. Zhu, J. Han, C. Gao, M. Liu, J.W. Song, Z.W. Wang, H.J. Li, Microstructures and mechanical properties of Al-Li 2198-T8 alloys processed by two different severe plastic deformation methods: A comparative study, Mater. Sci. Eng. A 681 (2017) 65–73, https://doi.org/10.1016/j.msea.2016.10.108.
[21] D. Orlov, Y. Beygelzimer, S. Synkov, V. Varyukhin, Z. Horita, Evolution of Microstructure and Hardness in Pure Al by Twist Extrusion, Mater. Trans. 49 (2008) 2–6 https://doi.org/10.2320/matertrans.ME200724.
[22] K. Edalati, D. Akama, A. Nishio, S. Lee, Y. Yonenaga, M. Jorge, Z. Cubero-Sesin, Horita, Influence of dislocation–solute atom interactions and stacking fault energy on grain size of single-phase alloys after severe plastic deformation using high-pressure torsion, Acta Mater. 69 (2014) 68–77, https://doi.org/10.1016/j.actamat.2014.01.036.
[23] Y. Huang, J.D. Robson, P.B. Prangnell, The formation of nanograin structures and accelerated room-temperature theta precipitation in a severely deformed Al–4 wt.% Cu alloy, Acta Mater. 58 (2010) 1643–1657, https://doi.org/10.1016/j.actamat.2009.11.008.
[24] W. Xu, X.C. Liu, X.Y. Li, K. Lu, Deformation induced grain boundary segregation in nanolaminated Al–Cu alloy, Acta Mater. 182 (2020) 207–214 https://doi.org/10.1016/j.actamat.2019.10.036.
[25] T. Masuda, X. Sauvage, S. Hirosawa, Z. Horita, Achieving highly strengthened Al–Cu–Mg alloy by grain refinement and grain boundary segregation, Mater. Sci. Eng. A 793 (2020) 139668 https://doi.org/10.1016/j.msea.2020.139668.
[26] S.V. Bobylev, N.A. Enikeev, A.G. Sheinerman, R.Z. Valiev, Strength enhancement induced by grain boundary solute segregations in ultrafine-grained alloys, Int. J. Plast. 123 (2019) 133–144 https://doi.org/10.1016/j.ijplas.2019.07.013.
[27] Y. Liu, M.P. Liu, X.F. Chen, Y. Cao, H. Roven, M. Murashkin, R.Z. Valief, H. Zhou Effect of Mg on microstructure and mechanical properties of Al-Mg alloys produced by high pressure torsion, Scr. Mater. 159 (2019) 137–141, https://doi.org/10.1016/j.scriptamat.2018.09.033.
[28] R.Z. Valiev, N.A. Enikeev, M.Yu. Murashkin, V.U. Kazykhanov, X. Sauvage, On the origin of the extremely high strength of ultrafine-grained Al alloys produced by severe plastic deformation, Scr. Mater. 63 (2010) 949–952, https://doi.org/10.1016/j.scriptamat.2010.07.014.
[29] N. Hansen, Hall-petch relation and boundary strengthening, Scr. Mater. 51 (2004) 801–806 https://doi.org/10.1016/j.scriptamat.2004.06.002.
[30] P. Donnadieu, Y. Shao, F. Geuser, G. Botton, S. Lazar, M. Cheynet, M. Boissieu, A. Deschamps, Atomic structure of T1 precipitates in AL-Li-Cu alloys revised with HAADF -STEM imaging and small-angle X-ray scattering, Acta Mater. 59 (2011) 462–472 https://doi.org/10.1016/j.actamat.2010.09.044.
[31] S. Zhang, W. Zeng, W. Yang, C. Shi, H. Wang, Ageing response of a Al–Cu–Li 2198 alloy, Mater. Des. 63 (2014) 368–374 https://doi.org/10.1016/j.matdes.2014.04.063.
[32] Z.M. Wang, G.J. Shiflet, Growth of δ on dislocations in a dilute Al-Li alloy, Metall. Mater. Trans. A. 29 (1998) 2073–2085 https://doi.org/10.1007/s11661-998-0033-1.
[33] B. Adamczyk, J. Mizera, K.J. Kurzydlowski, Thermal stability of model Al-Li alloys after severe plastic deformation-effect of the solute Li atoms, Mater. Sci. Eng. A 527 (2010) 4716–4722 https://doi.org/10.1016/j.msea.2010.04.032.
[34] C.C. Koch, A.R.O. Scattergood, K.A. Darling, J.E. Semones, Stabilization of nanocrystalline grain sizes by solute additions, J. Mater. Sci. 43 (2008) 7264–7272, https://doi.org/10.1007/s10853-008-2870-0.
[35] J. Li, J. Wang, G. Yang, On the stagnation of grain growth in nanocrystalline materials, Scr. Mater. 6 (2009) 945–948 https://doi.org/10.1016/j.scriptamat.2009.02.015.
[36] H. Jia, R. Bjorge, L. Cao, H. Song, K. Marthinsen, Y. Li, Quantifying the grain boundary segregation strengthening induced by Post-ECAP aging in an Al-5Cu alloy, Acta Mater. 155 (2018) 199–213 https://doi.org/10.1016/j.actamat.2018.05.075.
[37] R.Z. Valiev, F. Chmelik, F. Bordeaux, G. Kapelski, B. Baudelet, The Hall-Petch relation in submicro-grained Al-1.5% Mg alloy, Scr. Metall. Mater. 27 (1992) 855–860, https://doi.org/10.1016/0956-716X(92)90405-4.
[38] B. Noble, G.E. Thompson, T_1 (Al_2CuLi) precipitation in aluminum–copper–lithium alloys, Met Sci. 6 (1972) 167–174 https://doi.org/10.1179/030634572790445975.
[39] N. Nayan, S. Murty, A. Jha, B. Pant, S.C. Sharma, K. George, G. Sastry, Processing and characterization of Al–Cu–Li alloy AA2195 undergoing scale up production through the vacuum induction melting technique, Mater. Sci. Eng. A 576 (2013) 21–28 https://doi.org/10.1016/j.msea.2013.03.054.
[40] Y. Yan, L. Peguet, O. Gharbi, A. Deschamps, C.R. Hutchinson, S.K. Kairy, N. Birbilis, On the corrosion, electrochemistry and microstructure of Al–Cu–Li alloy AA2050 as a function of ageing, Materialia 1 (2018) 25–36, https://doi.org/10.1016/j.mtla.2018.05.003.